CHINESE OPTICS LETTERS

Vol. 19, No. 11 | November 2021

Chip-scale Brillouin instantaneous frequency measurement by use of one-shot frequency-to-power mapping based on lock-in amplification

Yuqiu Xu (徐雨秋), Yonglan Yang (杨涌澜), Xing Li (李 杏), Xin Wang (王 鑫), and Weiwen Zou (邹卫文)*

State Key Laboratory of Advanced Optical Communication Systems and Networks, Intelligent Microwave Lightwave Integration Innovation Center (imLic), Department of Electronic Engineering, Shanghai Jiao Tong University, Shanghai 200240, China

*Corresponding author: wzou@sjtu.edu.cn

Received August 30, 2021 | Accepted September 29, 2021 | Posted Online October 25, 2021

We demonstrate a chip-scale scheme of Brillouin instantaneous frequency measurement (IFM) in a CMOS-compatible doped silica waveguide chip. In the chip-scale Brillouin IFM scheme, the frequency-to-power mapping process is achieved by one-shot detection without additional time averaging and implemented by lock-in amplification, which successfully detects the Brillouin gain of the doped silica waveguide chip in the time domain. A Costas frequency modulated signal ranging from 8 GHz to 9 GHz is experimentally measured, and the frequency measurement errors are maintained within 58 MHz.

Keywords: instantaneous frequency measurement; stimulated Brillouin scattering; lock-in amplification; waveguide chip.
DOI: 10.3788/COL202119.113902

1. Introduction

An instantaneous frequency measurement (IFM) is aimed at detecting the frequency of unknown signals immediately in modern radar and electronic reconnaissance applications[1]. The traditional electronic IFM systems achieve excellent precision in a narrow band at the cost of expensive electronic components[2]. Recently, photonics-assisted IFM has made great progress in obtaining both large frequency measurement range and high frequency precision[3–6]. Considering the industrial applications, miniaturization and integration are inevitable trends. More and more studies are concentrated on chip-scale photonics-assisted IFM systems, mainly utilizing the nonlinearity of photonic components, such as micro-disk resonator (MDR) array[7], four-wave mixing in silicon waveguides[8], waveguide Bragg grating (WBG) filter[9], and Brillouin filter[10]. However, the medium used to engender the photonic effect always introduces a large loss (typically, > 10 dB). Recently, we proposed a new scheme of IFM based on stimulated Brillouin scattering (SBS), which owns a high potential for real-time detection[11]. However, the medium to generate the SBS effect is a long-length (2.6 km) dispersion compensating fiber (DCF), which is hardly suitable for miniaturization and integration. To realize a chip-scale Brillouin device, two essential requirements have been remarked in Ref. [12] for simultaneous confinement of the optical and acoustic waves. First, the effect of SBS should exceed other nonlinear phenomena, such as Kerr effect and Raman scattering. Second, the loss of devices should be smaller than the measurable Brillouin gain. Jiang *et al.* selected the As_2S_3 optical waveguide as the SBS medium because of its higher Brillouin gain coefficient than that of silica[10]. However, the As_2S_3 material is not compatible with CMOS, increasing the pressure on the manufacturing process. In contrast, we investigated the Brillouin properties of a doped silica waveguide chip based on a CMOS-compatible manufacturing technology[13]. It was found that the Brillouin gain coefficient ($24.6\ m^{-1}\cdot W^{-1}$) is two orders of magnitude greater than that of the silica optical fiber (SMF $0.215\ m^{-1}\cdot W^{-1}$) owing to the tight optical/acoustic confinement in the waveguide chip, although there are butt-coupling reflections, and the length of the waveguide is as short as ~1 m.

In this Letter, we present a new scheme to implement a chip-scale Brillouin IFM based on the SBS effect in a CMOS-compatible doped silica waveguide chip. Owing to the narrowband filtering effect of SBS, we change the center frequency of the Brillouin filter by frequency sweeping and obtain a one-shot frequency-to-power mapping curve, nominating the amplitude comparison function (ACF). Although the entire Brillouin gain of the doped silica waveguide chip is much smaller than that of long-length optical fibers, a lock-in amplifier is adopted to integrate the Brillouin gain of the waveguide chip in time domain and enhance the measurement accuracy. We successfully measure a Costas frequency modulated signal ranging from 8 GHz to 9 GHz with the measurement error of ~58 MHz.

© 2021 Chinese Optics Letters

2. Principle

SBS is a typical kind of phonon–photon interaction[14]. The pump lightwave and counter-propagating probe lightwave meet in an optical medium, and an acoustic field is stimulated. A part of the pump lightwave's power is transferred to the probe lightwave via the acoustic field, and the value of Brillouin gain is related to the beat frequency between the two lightwaves. A Lorentz curve, nominating the Brillouin gain spectrum (BGS), describes such a relationship. The full width at half-maximum (FWHM) of the BGS can be ~30 MHz in a silica optical fiber or ~120 MHz in a CMOS-compatible doped silica waveguide chip[13], which means an optical filter with a narrow band is naturally produced during SBS. The concept of the chip-scale Brillouin IFM via a lock-in amplifier is schematically illustrated in Fig. 1(a). SBS in the waveguide chip is generated by a traditional pump–probe configuration. Once the acoustic field is built by the interaction between the pump lightwave and counter-propagating probe lightwave, a part of the probe lightwave is amplified by the pump lightwave.

The amplitude of Brillouin gain (F_B) added to probe lightwave is described by

$$F_B = G_B I_P L_{\text{eff}}, \tag{1}$$

where G_B is the Brillouin gain coefficient determined by the physical characteristic of the SBS medium, I_P is the incident pump intensity, and L_{eff} is the efficient length of the SBS medium. Since the Brillouin gain is proportional to the efficient length, where the SBS interaction takes place, most previous SBS researches[15] are used to select long-length silica fibers as the SBS medium for the sake of achieving enough SBS interaction and enlarging the Brillouin gain. However, long-length fibers can scarcely satisfy the requirements of miniaturization and integration. Here, we employ a doped silica waveguide chip with the length of only 1 m as the SBS medium, leading to very weak Brillouin gain [at point b in Fig. 1(a)]. The output [$V_{\text{DO}}(\omega)$] of such an SBS interaction in the frequency domain[11] can be formulated by

$$V_{\text{DO}}(\omega) = E_P(\omega) \otimes G(\Delta\omega - \omega_B) + N(\omega), \tag{2}$$

where $E_P(\omega)$ is the pump spectrum, ω_B is the angular Brillouin shift frequency (BFS), $\Delta\omega$ is the beat frequency between the pump lightwave and probe lightwave, $G(\Delta\omega - \omega_B)$ is the BGS, and $N(\omega)$ is the noise spectrum. Without additional averaging processing, the Brillouin gain is submerged in the noise, and severe reflections are due to the butt coupling between the waveguide chip and the fiber pigtail, which is hard to measure directly. Here, a lock-in amplifier is adopted to suppress noise and integrate a weak signal [about nanovolts (nV)] in the time domain.

To play a role of the lock-in amplifier, a normal probe–pump configuration and signal settings should be adjusted. As depicted in Fig. 1(a), the pump lightwave is chopped by a square wave, which also functions as the reference signal of the lock-in amplifier. It was proved in Ref. [11] that a nonlinearly frequency sweeping pump signal can exert different response amplitudes since the dwell time of each pump frequency component varies from each other, and the accumulation of Brillouin gain is different. Here, the pump lightwave is also designed as a nonlinearly

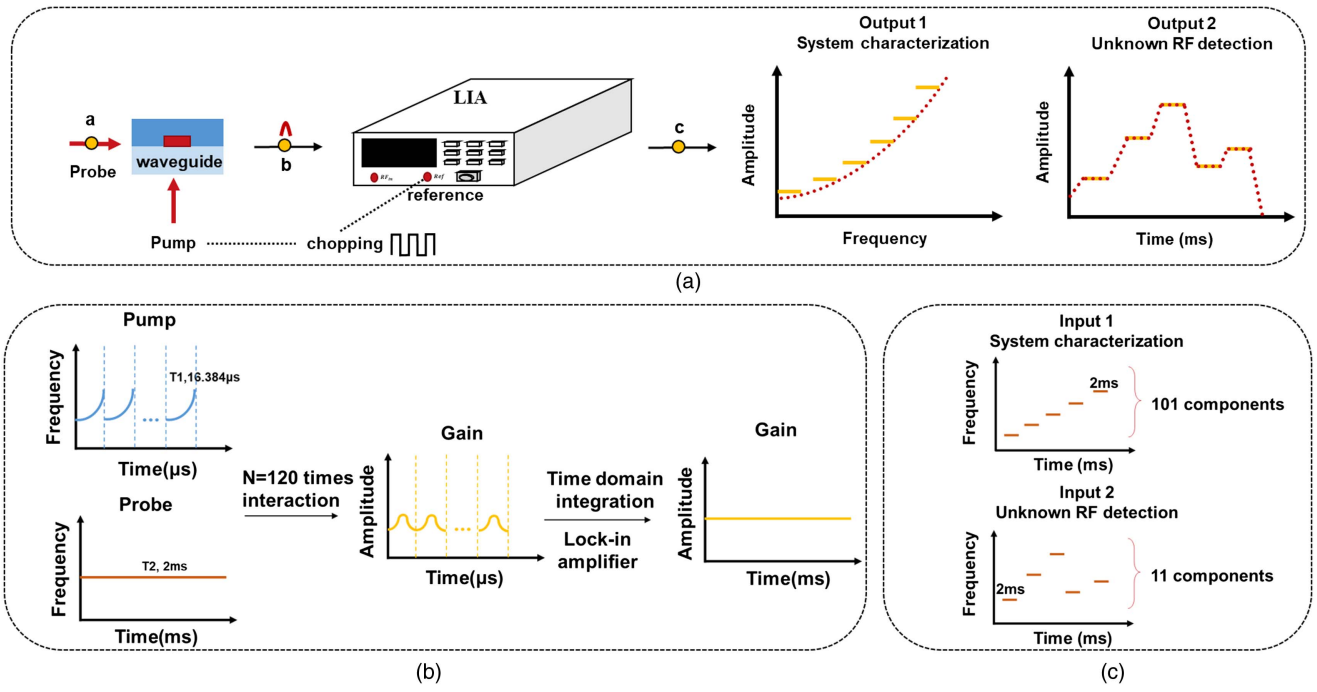

Fig. 1. (a) Schematic of the chip-scale Brillouin IFM via a lock-in amplifier (LIA). (b) Illustration of SBS interaction between the pump lightwave and probe lightwave. (c) Probe signal setting for system characterization and unknown RF detection based on the chip-scale Brillouin IFM.

frequency sweeping pulse with a period of ~16 μs. Due to the sampling rate of available arbitrary waveform generator (AWG) of 64 GSa/s, the longest signal generated by the AWG is ~16 μs. The dwell time of each probe frequency component is set to be 2 ms, which means it will interact with the local pump lightwave about 120 times. The signal settings provide a chance for the lock-in amplifier to accumulate enough Brillouin gain in the time domain to be measured.

Figure 1(b) illustrates more details of SBS interaction in the chip-scale Brillouin IFM configuration. The number of interactions (N) is determined by the dwell time of each probe frequency component (T_1) and the period of the pump signal (T_2), $N = [\frac{T_1}{T_2}]$. After about 120 times of interaction, a sequence of periodic Brillouin gain carried by probe lightwave appears in the time domain, which is also chopped by the reference signal. In principle, a lock-in amplifier makes use of a reference signal to accurately capture frequency components to be measured while ignoring others that are not synchronized with the reference signal[16]. The output after lock-in amplification of the Brillouin interaction at point c of Fig. 1(a) can be determined by

$$V_{\text{out}} = 120 \times \frac{1}{2} G_{\text{ac}} G_{\text{dc}} F_B E_0, \tag{3}$$

where G_{ac} is the voltage gain of the AC amplifier stage, G_{dc} is the voltage gain of the DC amplifier stage, and E_0 is the amplitude of the voltage controlled oscillator (VCO). It is shown that the output within an integration period of the lock-in amplifier is a DC signal, and the amplitude depends on two adjustable parameters: the DC gain and AC gain. The AC gain is determined by sensitivity of the lock-in amplifier, and the time constant determines the DC gain value. According to the following formula:

$$\begin{cases} \frac{8}{f_R} < T_C \le \frac{\sqrt{3}}{2\pi} \times \frac{1}{f_{s\max}} \\ \frac{8}{f_R} < T_C \le \frac{1}{2\pi} \times \frac{1}{f_{s\max}} \end{cases}, \tag{4}$$

where T_C is the time constant, f_R is the reference frequency, and $f_{s\max}$ is the highest frequency component of the detected signal, we can get the relationship

$$\begin{cases} f_R \ge 8 \times 2\pi f_{s\max} \approx 50 f_{s\max} \\ f_R \ge 8 \times \frac{2\pi}{\sqrt{3}} f_{s\max} \approx 29 f_{s\max} \end{cases}. \tag{5}$$

It indicates that f_R should be far greater than the highest frequency component of a slow-changing signal. The larger the T_C, the stronger the ability to suppress noise. But, the ability to detect fast-changing signals decreases. Considering that each frequency component of the probe lightwave lasts 2 ms, we set the frequency of reference signal as 1 MHz. Before we take an accurate measurement on the unknown microwave signal by the chip-scale Brillouin IFM system, a certain number of frequency components are programmed into a sequence with the same frequency interval and dwell time, as shown in Fig. 1(c) (Input 1). The final output is a monotonous frequency-to-power mapping curve even under a one-shot detection without any time-averaging processes, indicated as Output 1 in Fig. 1(a). Once the ACF curve is built, frequency measurement on the unknown signal is available through the power-to-frequency inversion method. Also depicted in Fig. 1(a), when the frequency distribution of the input signal is changed in the time domain (Input 2), we can get the power distribution of the output signal (Output 2) as well as the IFM of the input signal.

3. Experimental Setup

Figure 2 shows the experimental setup of the chip-scale Brillouin IFM scheme. A 1552 nm distributed-feedback laser diode (DFB-LD, NEL NLK1C6DAAA) is used as the light source, which is divided into two branches. The probe lightwave (upper branch) is modulated by the microwave signal to be measured or a certain linearly frequency sweeping signal [see Fig. 1(b)] for the ACF characterization via a carrier-suppressed single sideband electro-optic modulator (SSBM1, iXblue MXIQER-LN-30), and the lower sideband of SSBM1 is reserved. The pump lightwave (lower branch) is first modulated by the nonlinearly frequency sweeping signal via SSBM2. The peak-to-peak value of the signal is around 1 V, which determines the SBS modulation depth. The carrier attenuation of SSBM2 is set over 20 dB by adjusting the three DC bias voltages in case the residual carrier modulated by the reference signal generates serious pulse noises and decreases the Brillouin IFM accuracy. Different from the SSBM1, the upper sideband of the SSBM2 is reserved. It is noted that modulation of the two lightwaves to different sidebands enables a broader measurement range. The pump lightwave is chopped by a square wave (1 MHz) via an electro-optic modulator (EOM). Meanwhile, the chopping signal functions as the reference signal of the lock-in amplifier. The output of the erbium-doped fiber amplifier (EDFA1) is set as 14.5 dBm, and the output power of EDFA3 is set as 22 dBm. Two lightwaves with stationary power go through different circulators, respectively, and meet in the doped silica waveguide chip, where

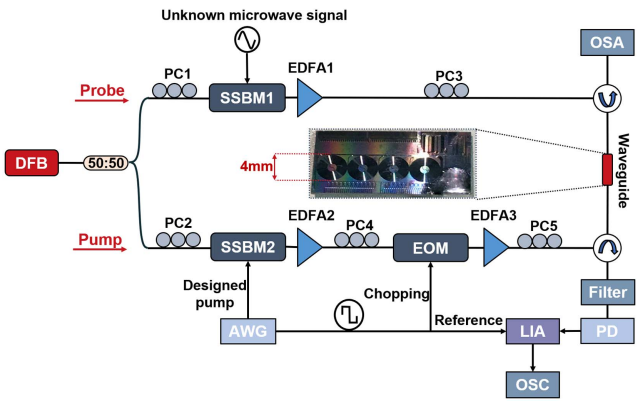

Fig. 2. Experimental setup of the chip-scale Brillouin IFM via a lock-in amplifier. DFB, distributed-feedback laser; SSBM, single sideband modulator; LIA, lock-in amplifier; AWG, arbitrary waveform generator; OSC, oscilloscope; OSA, optical spectrum analyzer.

SBS interaction is generated. Note that the waveguide (~1 m) is coiled into a disk-like shape, and the diameter is 4 mm. The optical filter (Alnair Labs, CVF-300CL) is placed before the photodetector to remove reflections of the pump lightwave due to the butt-coupling of the waveguide chip and the pigtails. A relatively pure probe sideband is reserved, coming into a photodetector with a narrow bandwidth (500 MHz). After it is converted into an electronic signal, the lock-in amplifier (Signal Recovery, Model 7280) is used to detect the weak Brillouin gain carried by the probe lightwave through integration in the time domain according to the reference signal.

4. Result and Discussion

The frequency of the pump lightwave sweeps continuously from 6.25 GHz to 7.25 GHz via an AWG (Keysight M9502A). Meanwhile, we encode the microwave generator (Keysight N5183B) to engender a sequence of 101 frequency components ranging from 8 GHz to 9 GHz. The frequency step is 10 MHz, and dwell time is set to be 2 ms. Note that the sensitivity of the lock-in amplifier is set to be 5 mV, and the AC gain is 34 dB. To attain a sharper system response, the time constant is set as 500 μs, which is shorter than the dwell time of the Costas frequency component. First, an experiment is carried out to acquire the BGS of the waveguide chip for more accurate measurement error analysis. The result shown in the inset of Fig. 3(a) indicates that the BFS of the waveguide chip is 15.24 GHz, and the FWHM of the BGS is about 120 MHz, which is broader than that of the DCF (~30 MHz) and means lower resolution of the Brillouin filter. Note that the following results are based on the measured BGS of the waveguide chip.

Figure 3(a) mainly presents the results of the one-shot frequency-to-power mapping curve. The solid curve shows the experimental data, and it is partially non-monotonous. The bending parts of the ACF curve are mainly caused by the fact that the integration time of the lock-in amplifier is not a strict integer multiple of the actual SBS interaction period. Besides, spontaneous Brillouin scattering (SpBS) concomitantly appears during SBS interaction and introduces fluctuation of the curve. In the non-monotonous area of the ACF, one certain power amplitude can be matched with several frequency components, causing large measurement errors. To compensate for the deficiency, we use the least-squares polynomial fitting method to fit the experimental data, which is shown in the dashed line of Fig. 3(a). It indicates that the ACF after curve fitting is monotonous but it introduces system errors somewhat.

We recode the microwave generator to engender a Costas frequency modulated sequence, consisting of 11 hopping frequency components with a dwell time of 2 ms. Note that normalization of output power is necessary when the hopping time of the Costas frequency modulated signal is larger than or lower than 2 ms. It should be mentioned again that the result is acquired through one-shot measurement without additional time averaging. Figure 3(b) depicts the Brillouin gain of the Costas frequency modulated signal, which is used for inversion of the frequency value. Note that the largest Brillouin gain value is below 15 mV, and most of the Brillouin gain values are below 5 mV. Lower Brillouin gain value means that the measurement results are more easily influenced by system noises. By comparing the received Brillouin gain value with the frequency-to-power mapping curve in Fig. 3(a), the IFM result and error analysis are illustrated in Fig. 4 and Table 1, respectively. Figure 4(a) indicates that the measured results match well with the nominal value, and the measurement error without the least-squares polynomial fitting is within 120 MHz, which is close to the FWHM of the BGS in the waveguide chip. The bending parts of the ACF curve are mainly distributed in the frequency zone of 8–8.5 GHz [see Fig. 3(a)], leading to relatively large measurement errors. The largest error appears at the frequency of

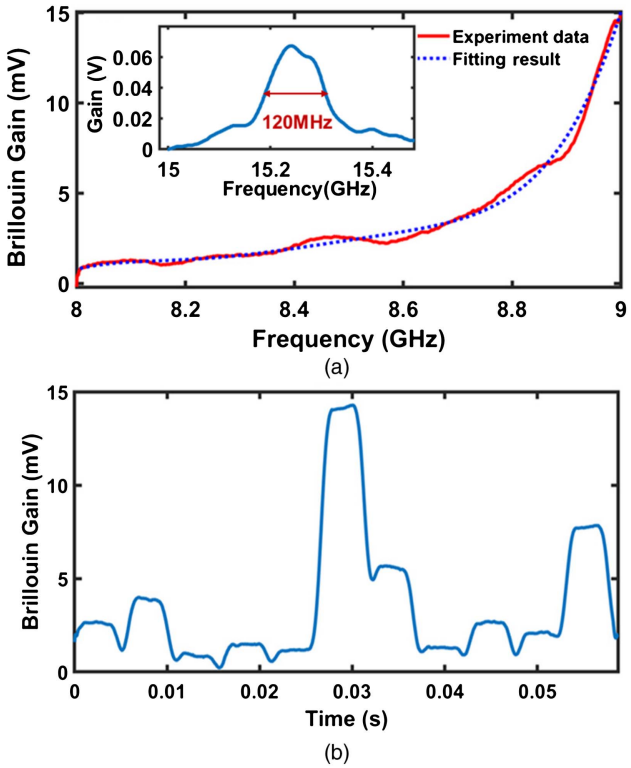

Fig. 3. (a) Frequency-to-power mapping curve for system characterization. (b) The Brillouin gain that a Costas frequency modulated signal carries.

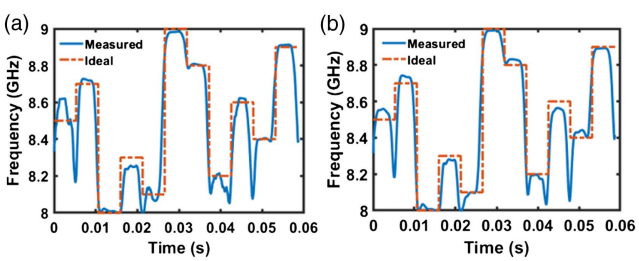

Fig. 4. Frequency measurement error analysis (a) without curve fitting and (b) with curve fitting.

Table 1. Costas Frequency Measurement Errors.

Frequency (GHz)	8.5	8.7	8.0	8.3	8.1	9.0	8.8	8.2	8.6	8.4	8.9
Error in Fig. 4(a) (MHz)	120	26	22	63	37	18	8	68	46	4	12
Error in Fig. 4(b) (MHz)	57	42	33	46	24	11	32	30	53	41	9

8.5 GHz. As mentioned above, we adopt the polynomial fitting to improve the measurement accuracy, and the kernel is to determine the best fitting coefficient. The larger the coefficient of the polynomial fitting is, the closer it is to the original curve distribution. The integer between 4 and 7 is a good choice for the least-squares polynomial fitting to optimize the original curve distribution. Figure 4(b) illustrates the best result of the polynomial fitting with the coefficient of five, where the measurement error is reduced from 120 MHz to 58 MHz. However, the measurement error of some frequency components, mostly ranging from 8.5 GHz to 9.0 GHz, increases. Note that the flatter the original ACF curve is, the more prominent the improvement on the Brillouin IFM accuracy is.

5. Conclusion

In conclusion, we have demonstrated a new scheme of chip-scale Brillouin IFM in a doped silica waveguide chip. Meanwhile, the chip-scale scheme can be totally achieved by a CMOS-compatible manufacturing process of the waveguide chip, silicon modulators, and silicon-germanium photodetectors. Although the Brillouin gain is still weak, the lock-in amplifier is adopted to accomplish one-shot frequency-to-power mapping through integration in the time domain without time averaging over signal periods. Theoretically, Brillouin IFM has the ability of cross-band frequency measurement if the bandwidth of modulators is wide enough. In this work, we select part of the X band to demonstrate the ability of the scheme. The Costas frequency modulated signal ranging from 8 GHz to 9 GHz is successfully measured, and the measurement errors are within 58 MHz. Note that the frequency precision of the chip-scale Brillouin IFM scheme is limited by the FWHM (120 MHz) of the SBS in the silica-doped waveguide chip, although it is enhanced slightly by the least-squares polynomial fitting. We might potentially achieve a higher precision of the Brillouin IFM if a waveguide chip with a narrower FWHW is employed.

Acknowledgement

This work was supported by the National Key Research and Development Program of China (No. 2019YFB2203700) and the National Natural Science Foundation of China (No. 61822508).

References

1. M. Skolnik, *Introduction to Radar Systems* (McGraw-Hill, 2001).
2. X. Zou, B. Lu, W. Pan, L. Yan, A. Stöhr, and J. Yao, "Photonics for microwave measurements," Laser Photon. Rev. **10**, 711 (2016).
3. D. Marpaung, "On-chip photonic-assisted instantaneous microwave frequency measurement system," IEEE Photon. Technol. Lett. **25**, 837 (2013).
4. B. Zhu, W. Zhang, S. Pan, and J. Yao, "High-sensitivity instantaneous microwave frequency measurement based on a silicon photonic integrated Fano resonator," J. Lightwave Technol. **37**, 2527 (2019).
5. D. Marpaung, J. Yao, and J. Capmany, "Integrated microwave photonics," Nat. Photon. **13**, 80 (2019).
6. Y. Zhou, F. Zhang, and S. Pan, "Instantaneous frequency analysis of broadband LFM signals by photonics-assisted equivalent frequency sampling," Chin. Opt. Lett. **19**, 013901 (2021).
7. Y. Chen, W. Zhang, J. Liu, and J. Yao, "On-chip two-step microwave frequency measurement with high accuracy and ultra-wide bandwidth using add-drop micro-disk resonators," Opt. Lett. **44**, 2402 (2019).
8. M. Pagani, B. Morrison, Y. Zhang, A. Casas-Bedoya, T. Aalto, M. Harjanne, M. Kapulainen, B. J. Eggleton, and D. Marpaung, "Low-error and broadband microwave frequency measurement in a silicon chip," Optica **2**, 751 (2015).
9. M. Burla, X. Wang, M. Li, L. Chrostowski, and J. Azaña, "Wideband dynamic microwave frequency identification system using a low-power ultracompact silicon photonic chip," Nat. Commun. **7**, 13004 (2016).
10. H. Jiang, D. Marpaung, M. Pagani, K. Vu, D. Choi, S. J. Madden, L. Yan, and B. J. Eggleton, "Wide-range, high-precision multiple microwave frequency measurement using a chip-based photonic Brillouin filter," Optica **3**, 30 (2016).
11. W. Zou, X. Long, X. Li, G. Xin, and J. Chen, "Brillouin instantaneous frequency measurement with an arbitrary response for potential real-time implementation," Opt. Lett. **44**, 2045 (2019).
12. B. J. Eggleton, C. G. Poulton, P. T. Rakich, M. J. Steel, and G. Bahl, "Brillouin integrated photonics," Nat. Photon. **13**, 664 (2019).
13. S. Li, X. Li, W. Zhang, J. Chen, and W. Zou, "Investigation of Brillouin properties in high-loss doped silica waveguides by comparison experiment," IEEE Photon. Technol. Lett. **32**, 948 (2020).
14. E. P. Ippen and R. H. Stolen, "Stimulated Brillouin scattering in optical fibers," Appl. Phys. Lett. **21**, 539 (1972).
15. K. Hu, L. Yi, W. Wei, and W. Hu, "Microwave photonic filter design and optimization based on stimulated Brillouin scattering using a directly modulated pump," Chin. Opt. Lett. **17**, 060603 (2019).
16. J. H. Scofield, "Frequency-domain description of a lock-in amplifier," Am. J. Phys. **62**, 129 (1994).